Neuronal dystonin isoform 2 is a mediator of endoplasmic reticulum structure and function

Scott D. Ryan[a,*], Andrew Ferrier[a,b,*], Tadasu Sato[a,c], Ryan W. O'Meara[a,b], Yves De Repentigny[a], Susan X. Jiang[d], Sheng T. Hou[d], and Rashmi Kothary[a,b,e]

[a]Ottawa Hospital Research Institute, Ottawa, ON K1H 8L6, Canada; [b]Department of Cellular and Molecular Medicine, University of Ottawa, Ottawa, ON K1H 8M5, Canada; [c]Division of Periodontology and Endodontology, Graduate School of Dentistry, Tohoku University, Sendai 980-8575, Japan; [d]Institute for Biological Sciences, National Research Council Canada, Ottawa, ON K1A 0R6, Canada; [e]Department of Medicine, University of Ottawa, Ottawa, ON K1H 8M5, Canada

ABSTRACT **Dystonin/Bpag1 is a cytoskeletal linker protein whose loss of function in dystonia musculorum (*dt*) mice results in hereditary sensory neuropathy. Although loss of expression of neuronal dystonin isoforms (dystonin-a1/dystonin-a2) is sufficient to cause *dt* pathogenesis, the diverging function of each isoform and what pathological mechanisms are activated upon their loss remains unclear. Here we show that dt^{27} mice manifest ultrastructural defects at the endoplasmic reticulum (ER) in sensory neurons corresponding to in vivo induction of ER stress proteins. ER stress subsequently leads to sensory neurodegeneration through induction of a proapoptotic caspase cascade. *dt* sensory neurons display neurodegenerative pathologies, including Ca^{2+} dyshomeostasis, unfolded protein response (UPR) induction, caspase activation, and apoptosis. Isoform-specific loss-of-function analysis attributes these neurodegenerative pathologies to specific loss of dystonin-a2. Inhibition of either UPR or caspase signaling promotes the viability of cells deficient in dystonin. This study provides insight into the mechanism of *dt* neuropathology and proposes a role for dystonin-a2 as a mediator of normal ER structure and function.**

Monitoring Editor
Paul Forscher
Yale University

Received: Jun 27, 2011
Revised: Oct 26, 2011
Accepted: Dec 12, 2011

INTRODUCTION

The eukaryotic cytoskeleton comprises three cytoskeletal networks, including microtubules, actin microfilaments, and intermediate filaments. These filaments rely on cytoskeletal cross-linking proteins to facilitate their multifaceted functions, ranging from vesicular transport and maintenance of organelle integrity to mitosis (Fuchs and Karakesisoglou, 2001). As such, loss of cytoskeletal-linking proteins can have grave implications on cellular functioning and viability (Sonnenberg and Liem, 2007). In particular, loss of the neuronal cytoskeletal linking protein dystonin has been attributed to degeneration of both sensory and motor neurons (Brown *et al.*, 1995; Guo *et al.*, 1995; De Repentigny *et al.*, 2011).

Dystonia musculorum (*dt*) is an inherited homozygous recessive sensory neuropathy caused by mutations in the dystonin gene (*Dst*; Duchen *et al.*, 1964). At approximately 2 wk postnatal development, *dt* mice exhibit loss of control of the fore limbs, hind limbs, and trunk, and they die shortly thereafter of unknown causes (Duchen, 1976). Several *dt* alleles exist through spontaneous mutations (dt^{27}), chemically induced mutations, targeted alleles (dt^{tm1Efu}), and transgenic insertions (dt^{Tg4}; Pool *et al.*, 2005). Although only three *dt* mutations (dt^{Tg4}, dt^{tm1Efu}, and dt^{Alb}) have been characterized at the DNA level, dt^{Tg4} and dt^{27} are allelic and do not complement (Kothary *et al.*, 1988; Guo *et al.*, 1995). To date, *dt* pathologies have been recorded in motor neurons, skeletal muscle, and Schwann cells, but degeneration is most prominent in the sensory neurons of the dorsal root ganglia (DRG; Dowling *et al.*, 1997; Bernier *et al.*, 1998; Dalpe *et al.*, 1999; De Repentigny *et al.*, 2011).

The *Dst* gene is exceptionally large (~400 kb in mice) and gives rise to three tissue-specific dystonin isoforms—dystonin-e (epithelial isoform, ~315 kDa), dystonin-b (muscle isoform, ~834 kDa), and

This article was published online ahead of print in MBoC in Press (http://www.molbiolcell.org/cgi/doi/10.1091/mbc.E11-06-0573) on December 21, 2011.

*These authors contributed equally to this work.

Address correspondence to: Rashmi Kothary (rkothary@ohri.ca).

Abbreviations used: DMC, dynein motor complex; DRG, dorsal root ganglia; DRGN, DRG sensory neuron; Dst, dystonin gene; dt, dystonia musculorum; MACF1b, microtubule actin cross-linking factor-1b; TdT, terminal deoxynucleotidyl transferase; UPR, unfolded protein response.

dystonin-a (neuronal isoform, ~615 kDa; Sawamura *et al.*, 1991; Brown *et al.*, 1995; Leung *et al.*, 2001; Okumura *et al.*, 2002). Whereas dystonin-e serves as an autoantigen in the skin blistering disease bullous pemphigoid, loss of function of the dystonin-a isoform or isoforms is causal in the *dt* disorder (Kothary *et al.*, 1988; Sawamura *et al.*, 1991; Brown *et al.*, 1995; Pool *et al.*, 2005). Like muscle, three major neuronal isoforms are derived through alternative splicing, namely dystonin-a1, dystonin-a2, and dystonin-a3 (Young and Kothary, 2007). These isoforms share an N-terminal actin-binding domain, an extensive coiled-coil region, and a C-terminal microtubule-binding domain, allowing for interactions with cytoskeletal filaments (Leung *et al.*, 2001). Although the dystonin-a isoforms share similar domain architecture, it is the unique N-terminal regions that differentiate them and dictate their subcellular localization. Specifically, dystonin-a1 encodes a short N-terminal domain that includes an actin-binding domain, whereas dystonin-a2 possesses a transmembrane domain and dystonin-a3 possesses a putative myristoylation domain, aiding their membrane localization to the nuclear envelope and perinuclear membranes and to the plasma membrane, respectively (Jefferson *et al.*, 2006; Young *et al.*, 2006). Recently it has been demonstrated that the lack of one copy of the *Dst* gene or the presence of truncated forms of the mutant protein in humans can lead to a partial disorganization of the sensory and motor circuits. Giorda and collaborators described a human subject with a translocation in the *Dst* gene that specifically disrupted neuron- and muscle-specific isoforms and was associated with a profound delay in the acquisition of cognitive and motor skills, as well as in visual maturation (Giorda *et al.*, 2004). Thus, although no mutations in *Dst* have been identified in humans, haploinsufficiency or altered expression can result in phenotypic abnormalities reminiscent of the inherited disorder in mice.

A common cellular pathology preceding *dt* sensory neuron degeneration is axonal swelling, characterized by the accumulation of organelles and vacuoles within *dt* sensory neurons (Janota, 1972). These accumulations are accompanied by disorganized neurofilament, actin and microtubule networks in *dt* sensory neurons (Yang *et al.*, 1996, 1999; Leung *et al.*, 1999a), which in turn lead to bidirectional impairment of fast axonal transport (Dalpe *et al.*, 1998; De Repentigny *et al.*, 2003). Although neurofilament defects do exist in *dt* mice, they are not causal in initiation of *dt* pathology (Bernier and Kothary, 1998; Eyer *et al.*, 1998). Moreover, the microtubule cytoskeleton of *dt* and wild-type (WT) sensory neurons grown in culture displays no ultrastructural defects, and local trafficking of mitochondrial organelles proceeds normally (Pool *et al.*, 2006). Nonetheless, enhanced apoptosis is observed in these cultures (Pool *et al.*, 2006). Consequently, it is plausible that abnormalities aside from axonal cytoskeleton defects may initiate or contribute to *dt* sensory neuron pathology. Some studies suggest that the dystonin-a2 isoform is involved in nuclear envelope structuring, nuclear tethering, and organization of membranous structures surrounding the nucleus (Young *et al.*, 2003, 2006; Young and Kothary, 2008). Indeed, dt^{Tg4} sensory neurons (devoid of dystonin-a1 and dystonin-a2 expression) display perikaryal defects and show altered expression of the microsomal enzyme protein disulfide isomers (Young and Kothary, 2008). Yet the mechanism resulting in perikaryal defects in *dt* remains uncertain. Taken together, the observations make it reasonable to presume that dystonin-a has a role in maintaining integrity of the ER and nuclear envelope, and subsequently organelle function, but this hypothesis has yet to be empirically validated.

Whereas *dt* pathology has been thoroughly examined, there remains a dearth of evidence to explain the mechanisms mediating *dt* pathogenesis. Moreover, although it is known that the dt^{Tg4} mouse strain is devoid of dystonin-a1 and dystonin-a2 expression, it is unresolved as to whether loss of a single isoform or combination of isoforms is responsible for neurodegeneration. The present study therefore aims to elucidate underlying mechanisms of *dt* pathogenesis and to determine the individual roles of dystonin-a1 and dystonin-a2 in *dt* sensory neuronal degeneration. To this extent, we selectively reduced the expression of dystonin-a1 or dystonin-a2 via small interfering RNA (siRNA) in F11 neuronal cells and screened these cells for canonical endoplasmic reticulum (ER) stress proteins and caspase activity and assessed cell viability using various cell death assays. In parallel, dt^{27} DRGs and primary sensory neurons were screened for ER stress, caspase activation, and sensory neuron viability using similar experimental analysis. To assess *dt* ER integrity and function, ultrastructural and ratiometric Ca^{2+} analyses were conducted, respectively. Data presented here provide insight into the mechanisms underlying neuropathology in *dt* mice. Furthermore, this study proposes a novel role for dystonin-a2 as a critical structural component of perinuclear organelles, required for maintenance of ER homeostasis.

RESULTS

Loss of dystonin-a2 leads to activation of a neurodegenerative caspase cascade in dystonia musculorum mice

To evaluate the isoform-specific contribution of dystonin loss to neurodegeneration in *dt* mice, we first evaluated the correlation between degeneration of sensory neurons and phenotypic onset in dt^{27} mice, which are null for all three neuronal isoforms of dystonin. At the prephenotype stage (P4), DRGs from WT and dt^{27} mice were negative for both Fluoro-Jade B staining and terminal transferase dUTP nick-end labeling (TUNEL; Figure 1, A, B, E, and F), indicating the absence of neurodegeneration. In phenotypic (P15) dt^{27} animals, however, a marked increase in both Fluoro-Jade staining and TUNEL labeling (Figure 1, C, D, G, and H) was observed relative to WT littermates. This result indicates that phenotypic onset correlates closely with severe degeneration of DRG sensory neurons. We then sought to determine which neuronal isoform of dystonin was critical to maintaining cell viability in sensory neurons. dt^{Tg4} transgenic mice are null for dystonin-a1 and dystonin-a2 but express dystonin-a3 (Pool *et al.*, 2005). Labeling of P15 WT and dt^{Tg4} DRGs for TUNEL shows an increase in TUNEL reactivity in dt^{Tg4} DRGs relative to WT (Supplemental Figure S1). This indicates that the neurodegeneration associated with dystonin loss in dt^{Tg4} mice is not due to loss of dystonin-a3 but rather to loss of dystonin-a1 or dystonin-a2 or the combined loss of both.

The diverging cellular localization of dystonin-a1 and dystonin-a2 resulting from the heterogeneity of the N-terminus would implicate distinct organelle-specific dysfunction with their depletion (Young and Kothary, 2008). To determine the functional requirement of both dystonin-a1 and dystonin-a2 to neuronal viability, we performed isoform-specific loss-of-function analysis in immortalized F11 neuronal culture. F11 neuronal cells are a fusion of embryonic rat DRG neurons with mouse neuroblastoma cells. The resulting hybrid exhibits neuronal gangliosides, action potentials, and extensive neurite-like processes (Platika *et al.*, 1985). We first assessed the efficiency of isoform-specific, siRNA-mediated dystonin knockdown. In the absence of isoform-specific dystonin antibodies, we assessed knockdown of exogenously expressed dystonin-a1–green fluorescent protein (GFP) and dystonin-a2–yellow fluorescent protein (YFP) fusion proteins coupled to siRNA-mediated knockdown of endogenously expressed dystonin-a1 and dystonin-a2 mRNA (Figure 2, A

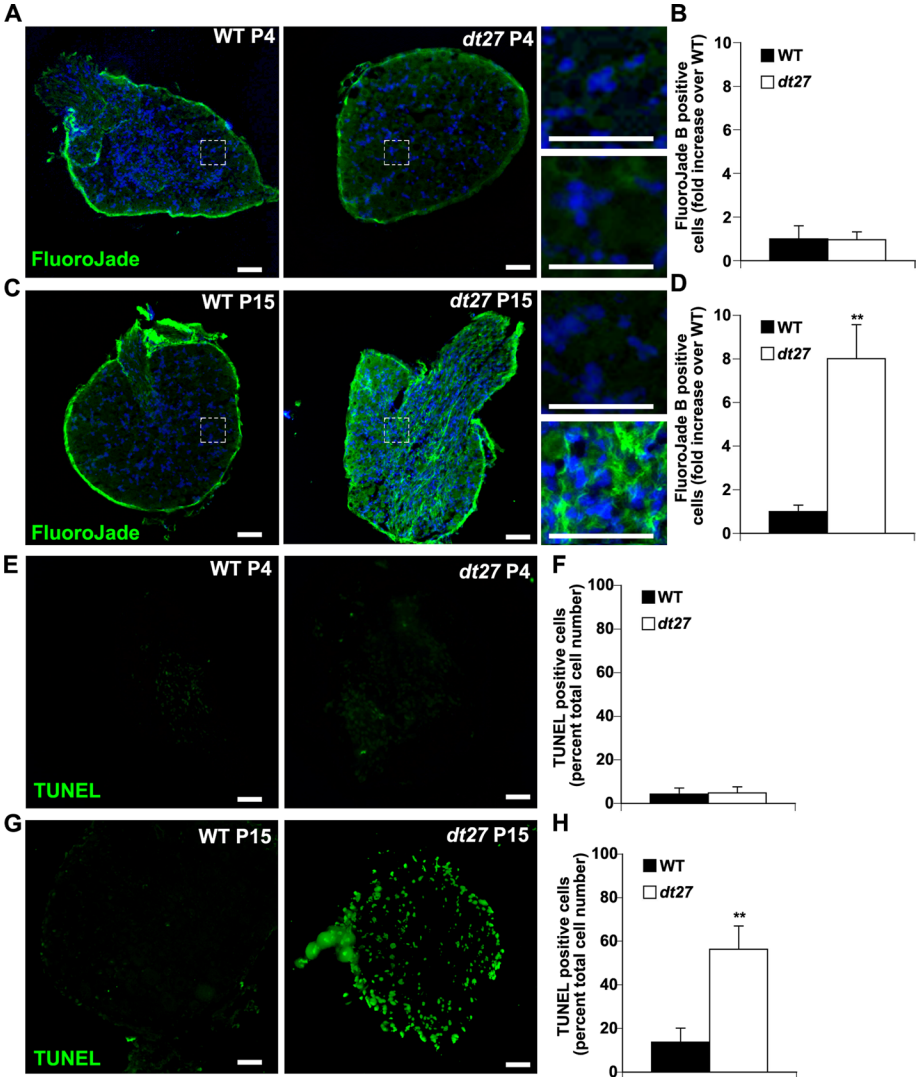

FIGURE 1: Dystonin deficiency leads to degeneration of sensory neurons in mice. DRGs from P4 (A, B) and P15 (C, D) WT and *dt*^{27} mice were stained with Fluoro-Jade B to identify degenerating neurons. No degeneration of sensory neurons is evident prephenotype (A, B), whereas Fluoro-Jade–positive degenerating neurons were evident at P15 in phenotypic *dt*^{27} animals (C, D). Analysis of TUNEL labeling from P4 (E, F) and P15 (G, H) WT and *dt*^{27} DRGs yielded no difference in apoptotic index prephenotype (E, F). At P15, a significant increase in percentage TUNEL-positive cells was observed in phenotypic *dt*^{27} animals relative to WT controls (G, H). Scale bars, 50 μm; Student's *t* test, **$p < 0.01$, $n = 5$.

and B, and Supplemental Figure S2, A and B). siRNA-mediated targeting of dystonin proved to be isoform specific. Analysis of the effect of dystonin loss on neuronal viability showed that knockdown of dystonin-a2 resulted in an increase in death within 24 h as indicated by ethidium homodimer incorporation (Figure 2C and Supplemental Figure S2C) and an increase in TUNEL labeling within 48 h (Figure 2D) of silencing relative to scrambled control. Loss of dystonin-a1 has no impact on cell death (Figure 2, C and D, and Supplemental Figure S2C). Positive TUNEL labeling in phenotypic DRGs from *dt*^{27} mice coupled with TUNEL labeling following specific depletion of dystonin-a2 in F11 neuronal cells led us to explore the pathway of apoptotic induction in order to trace to the mechanism of pathology.

We thus screened for caspase activation in F11 cells following siRNA-mediated depletion of dystonin isoforms. Using fluorescence-labeled inhibitors of caspase activity, we screened F11 neuronal cells for activation of caspases 2, 12, 8, and 3 at multiple time points following loss of either dystonin-a1 or dystonin-a2 (Figure 3). No induction of death receptor–associated caspase 8 was detected (Figure 3A), thus excluding the extrinsic apoptotic cascade as a potential mediator of death. A pronounced increase in both caspase 2 and caspase 3 activity was observed (Figure 3, C and D) following 24 and 48 h of dystonin-a2 depletion relative to scrambled siRNA control cells, coupled to a modest increase in caspase 12 activation (Figure 3B) following 48 h of dystonin-a2 depletion. Loss of dystonin-a1, however, had no effect on caspase activation. Collectively, these data strongly suggest that specific depletion of dystonin-a2 induces an intrinsic apoptotic cascade that is a likely effector of neurodegeneration in *dt*.

Loss of dystonin results in ER stress–mediated induction of the unfolded protein response

To ascertain the cellular stresses evoking the increase in caspase activity in F11 neuronal cells, we first discerned which if any of these caspases contributed to pathology in *dt*^{27} mice by screening WT and *dt*^{27} primary sensory neurons for caspase activation. A time course of caspase 3 activation was conducted in DRG sections at P4, P10, and P15 (Figure 4A). These data suggest that caspase 3 activation in DRGs coincides with phenotypic onset in *dt*^{27} mice. We then established the ability of these neurons to survive in culture. Cultured DRG sensory neurons (DRGNs) from P4 and P15 WT and *dt*^{27} mice were assessed by TUNEL (Figure 4B). Whereas both WT and *dt*^{27} cultures were negative for TUNEL labeling at P4 (Figure 4C), we were surprised to see that P15 DRGNs from *dt*^{27} mice also showed no increase in TUNEL labeling relative to WT controls (Figure 4D). We then screened P15 WT and *dt*^{27} sensory neurons for caspase activation (Figure 4E). Although we saw no induction of death receptor–associated caspase 8 and no significant increase in ER-associated caspase 12 activity, an increase in activity of executioner caspases 2 and 3 was observed. Activation of caspase 2 in whole DRGs was confirmed by Western analysis of cleaved (active) caspase 2 at P4 (Figure 4, F and G) and P15 (Figure 4, F and H). Caspase activation was only observed in DRGs from phenotypic *dt*^{27} mice (Figure 4, F and H). In addition, although these results suggest that culturing sensory neurons at a phenotypic stage selects for those neurons that have not yet undergone apoptosis, a caspase 2–dependent signaling cascade has nonetheless been initiated.

In rodents, ER stress leading to neuronal loss is mediated in part by activation of caspase 12 (Nakagawa *et al.*, 2000). Caspase 2, however, has been proposed as a functional orthologue to caspase 12 in some systems, mobilized in response to ER stress to activate downstream caspase 3/7 (Hitomi *et al.*, 2004; Cheung

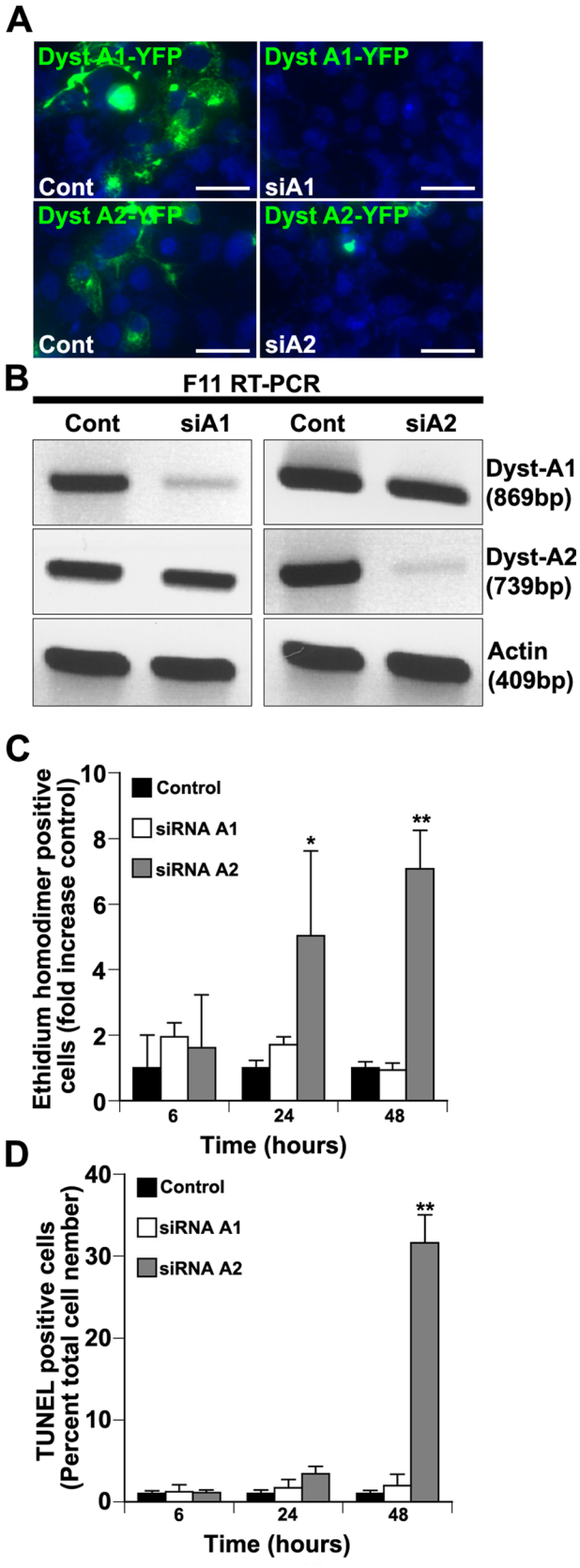

FIGURE 2: Isoform-specific loss of dystonin-a2 promotes neuronal cell death. (A) Efficiency of siRNA-mediated knockdown of exogenously expressed dyst-a1–YFP and dyst-a2–YFP protein was evaluated in COS-1 cells by epifluorescence. (B) Efficiency of siRNA-mediated knockdown of endogenously expressed dystonin-a1 and dystonin-a2 mRNA was measured in F11 neuronal cells by RT-PCR. Knockdown of dystonin-a2 resulted in an increase in death as assessed by ethidium homodimer incorporation within 24 h (C) and an increase in TUNEL labeling within 48 h of silencing relative to scrambled control. Loss of dystonin-a1 has no impact on cell death (C, D). Scale bars, 10 μm; ANOVA, post hoc Dunnett's *t* test, *$p < 0.05$, **$p < 0.01$, $n = 5$.

et al., 2006). Caspase 2 localizes to both the Golgi apparatus and ER (Mancini *et al.*, 2000; Ferri and Kroemer, 2001; Cheung *et al.*, 2006). Activation is associated with fatal interruption of protein transport from the ER to the Golgi, triggering cell death (Murakami *et al.*, 2007; Ouasti *et al.*, 2007). To evaluate whether caspase 2 was localized to the ER and functioning as a component of ER stress following dystonin loss, we contrasted caspase 2 localization in F11 neuronal cells between the ER and Golgi and determined whether dystonin-a2 depletion altered this localization (Figure 5). Confocal analysis of caspase 2 with the ER marker calreticulin-YFP showed extensive colocalization (Figure 5A). Furthermore, loss of dystonin-a2 has no effect on the distribution of caspase 2 in the ER (Figure 5, B and E). Assessment of caspase 2 colocalization with Golgi-YFP also showed caspase 2 present in Golgi (Figure 5C). Consistent with our findings in the ER, loss of dystonin-a2 has no effect on Golgi-localized caspase 2 (Figure 5, D and F). Although dystonin-a2 has no effect on overall caspase 2 distribution, we see extensive caspase 2 staining through both the ER and Golgi complex, suggesting that caspase 2 is positioned in F11 neuronal cells to respond to ER stress signals. We thus examined the effect of dystonin-a2 depletion on the macrostructural organization of the ER. It was surprising that staining of endogenous calreticulin in F11 neuronal cells showed no obvious aberrations in ER macrostructure (Figure 5G).

Further elucidation of the ER stress mechanism associated with neurodegeneration in dt^{27} mice focused on two canonical ER stress signal transduction cascades—mobilization of ER Ca^{2+} stores and the unfolded protein response (UPR). Phenotypic WT and dt^{27} DRGs were analyzed by Western blot for induction of chaperones of protein folding—BiP (GRP78) and CHOP (GADD153). Induction of these proteins is an early marker of ER stress (Gulow *et al.*, 2002). Expression of these proteins increases following cessation of translation induced by UPR activation (Munro and Pelham, 1986; Gulow *et al.*, 2002). A significant induction of both BiP and CHOP was observed in DRGs from phenotypic dt^{27} mice relative to WT (Figure 6, A–C). Isoform-specific depletion of dystonin was subsequently performed to ascertain which dystonin isoform is critical to ER function. Western and immunofluorescence analysis of F11 neuronal cells revealed an increase in BiP and CHOP expression within 48 h of dystonin-a2 silencing but not following dystonin-a1 silencing (Figure 6, D–I). UPR signal transduction results in the mRNA splicing of XBP1 by IRE1 (Yoshida *et al.*, 2001). Translation of spliced XBP1 mRNA, a potent transcription factor, induces BiP and CHOP expression (Lee *et al.*, 2003). UPR-mediated activation of XBP1 splicing was determined following isoform-specific depletion of dystonin. Although dystonin-a1 depletion resulted in a modest induction of XBP1 splicing, a dramatic increase in splicing was observed following loss of dystonin-a2 (Figure 6, J and K). Collectively, these data demonstrate that dystonin-a2 functional loss is the predominant mediator of neurodegeneration in dt^{27} mice through induction of an ER stress–mediated apoptotic cascade.

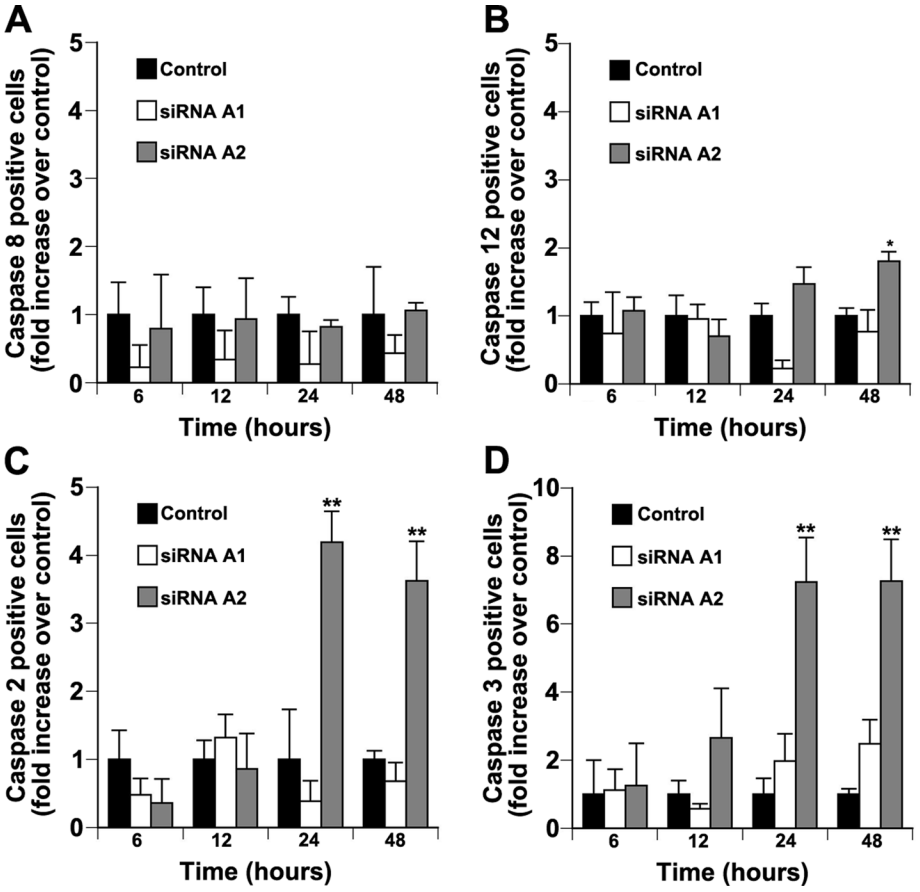

FIGURE 3: Loss of neuronal dystonin-a2 results in activation of a caspase 2–dependent caspase cascade in F11 cells. F11 neuronal cells were screened for caspase activation using FLICA assays at multiple time points following knockdown of either dystonin-a1 or dystonin-a2. (A) No induction of death receptor–associated caspase 8 was observed at any time point. (B) A modest increase in caspase 12 activation was measured following 48 h of dystonin-a2 depletion. A pronounced increase in both caspase 2 (C) and caspase 3 (D) activity was observed following 24 and 48 h of dystonin-a2 depletion relative to scrambled siRNA control cells. Loss of dystonin-a1 had no effect on caspase activation (A–D). ANOVA, post hoc Dunnett's *t* test, *p < 0.05, **p < 0.01, n = 5.

ER structural integrity and calcium homeostasis are perturbed in *dt*^{27} mice

We previously reported that the N-terminal transmembrane domain of dystonin-a2 localizes the protein to the ER and that overexpression of dystonin-a2 results in reorganization of ER membranes (Young and Kothary, 2008). We thus postulated that ER stress induced by loss of the dystonin-a2 isoform might manifest as a result of perturbed cytoarchitecture within the ER and/or the impaired anchoring of ER membrane to the cytoskeleton. To test these possibilities further, we performed a time course of electron microscopy on WT and *dt*^{27} DRGs and evaluated ER morphology within sensory neurons (Figure 7, A–C). Normal striated patterning of ER can be identified in WT and *dt*^{27} DRGs at P4; however, by P10 the ER of *dt*^{27} DRGs appear dilated. This pathology increases in severity by P15, and in some instances the ER appears vacuolated, suggesting impaired ER cytoskeletal dynamics (Figure 7D). This ER pathology precedes phenotypic onset in *dt*^{27} mice.

We then evaluated whether a defect in ER morphology correlates with aberrant Ca^{2+} homeostasis, thus initiating ER stress signal transduction. WT and *dt*^{27} primary sensory neurons were visualized and recorded using the Ca^{2+}-sensitive dye Fura-2AM. Neurons were depleted of Ca^{2+} by perfusion in Ca^{2+}-free tyrode solution. Cells were then stimulated with caffeine to promote ryanodine receptor–mediated Ca^{2+} efflux from the ER (Ehrlich *et al.*, 1994). *dt*^{27} sensory neurons showed reduced ER calcium efflux relative to WT sensory neurons as indicated by a reduction in maximum peak amplitude following caffeine administration (Figure 7, E–G). Ca^{2+} reuptake was normal in both WT and *dt*^{27} sensory neurons as indicated by the second peak response following caffeine administration. To confirm that the observed peak response was indeed a result of Ca^{2+} efflux from the ER, following caffeine administration, neurons were perfused for 3 min with thapsigargin to block Ca^{2+} reuptake by sarco/endoplasmic reticulum Ca^{2+}-ATPase (SERCA) pumps (Lytton *et al.*, 1991). Following SERCA inhibition, caffeine stimulation did not result in Ca^{2+} mobilization, confirming that caffeine was indeed stimulating efflux from ER stores alone and that all Ca^{2+} in the ER was effluxed following stimulation with caffeine (Figure 7, H and I). We then further evaluated which dystonin isoform was primarily responsible for maintaining ER Ca^{2+} homeostasis. Mobilization of ER Ca^{2+} stores was measured following isoform-specific dystonin silencing in F11 neuronal cells (Supplemental Figure S3). Isoform-specific loss of dystonin-a2 resulted in a decrease in maximum peak amplitude relative to control siRNA-treated cells, whereas dystonin-a1 depletion had no effect on ER Ca^{2+} efflux (Supplemental Figure S3, A–D). Taken together, these data suggest that impaired cytoarchitecture at the ER results in ER dilation and a reduction in the steady-state levels of ER Ca^{2+}. This in turn would promote the observed ER stress–mediated apoptotic signaling cascade.

Inhibition of ER stress signal transduction rescues dystonin-deficient neurons from death

Finally, to confirm that ER stress was the primary source of neuronal degeneration in *dt*^{27} mice, we attempted to rescue neurons from cell death by intervening in the apoptotic signal cascade identified (Figure 8). We first assessed whether various caspase inhibitors could prevent downstream executioner caspase 3 activation in F11 neuronal cells following loss of dystonin-a2. Pan-caspase inhibition or inhibition of caspase 2 but not caspase 12 prevented downstream caspase 3 activation in F11 neuronal cells (Figure 8A). This was confirmed in primary sensory neurons from *dt*^{27} mice, in which pan-caspase inhibition in addition to inhibition of either caspase 2 or caspase 12 prevented downstream caspase 3 activation (Figure 8B). These data confirmed that ER-associated caspase activation is critical to neurodegeneration in *dt*^{27}. We then sought to block UPR signal transduction directly and evaluate the effect on cell viability. Salubrinal is a selective inhibitor of cellular complexes that dephosphorylate eIF2α, a downstream effector of UPR-mediated protein kinase R–like ER kinase (PERK) activation (Boyce *et al.*, 2005).

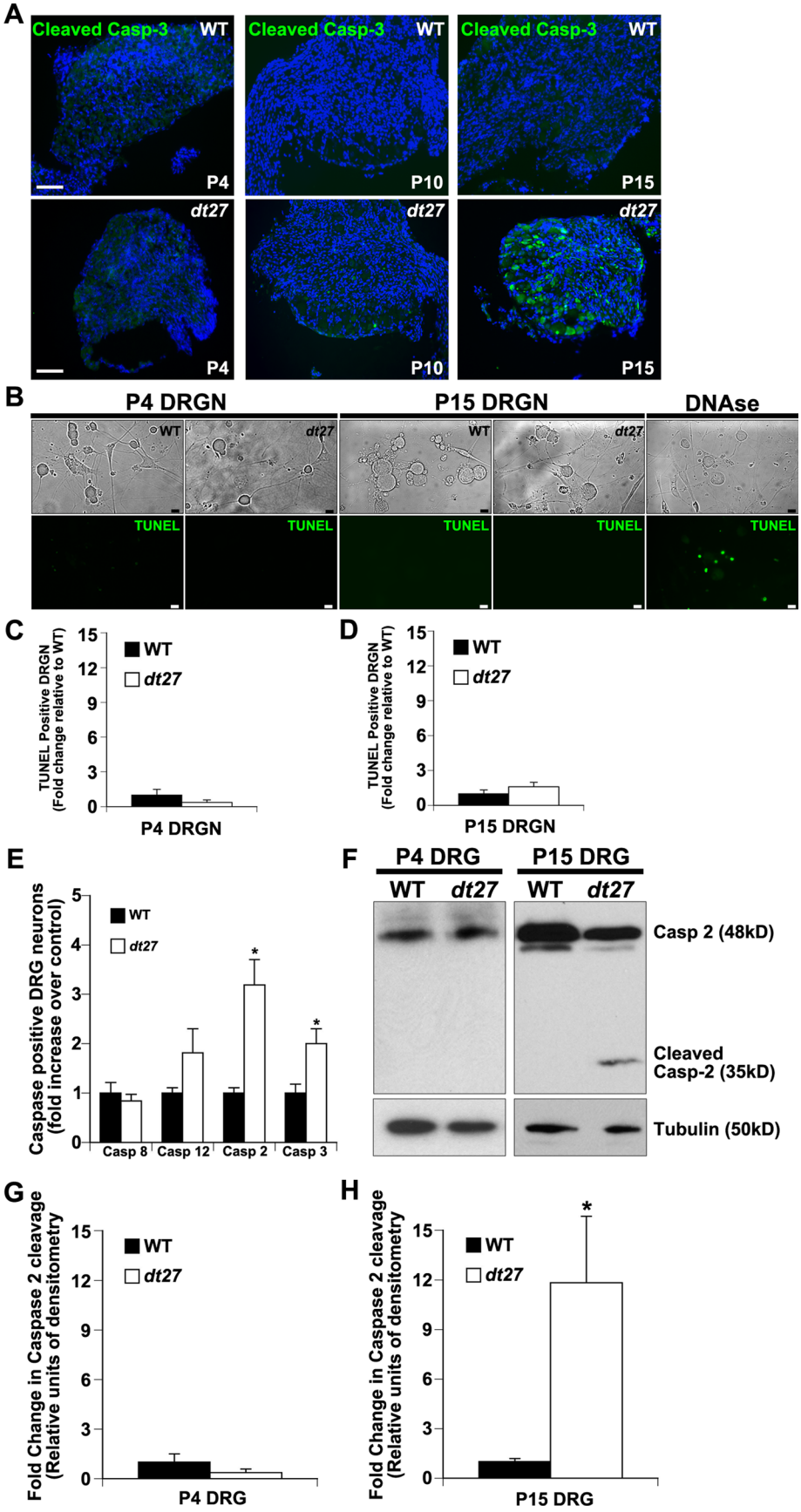

FIGURE 4: Loss of dystonin results in activation of an ER-associated caspase cascade in DRGs. (A) A postnatal time course of caspase 3 activity was conducted by immunofluorescence analysis of cleaved caspase 3 expression at P4, P10, and P15 in WT and *dt*^{27} DRG sections; scale bars, 50 μm. (B) Survival of cultured primary sensory neurons was then assessed by TUNEL labeling of WT and *dt*^{27} DRGNs at P4 and P15; scale bars, 10 μm. DNase-treated sensory neurons were processed as a positive control. Fold change in TUNEL reactivity was quantified at (C) P4 and (D) P15. Data are expressed as fold increase in TUNEL-positive *dt*^{27} neurons relative to WT; Student's *t* test, n = 3–6. (E) WT and *dt*^{27} primary sensory neurons were screened for caspase activation following 48 h in culture using FLICA assays. Although no induction of death receptor–associated caspase 8 was measured, an increase in activity of executioner caspases 2 and 3 was recorded; ANOVA, post hoc Dunnett's *t* test, *$p < 0.05$, n = 9. (F) Caspase 2 activity was confirmed by Western analysis of pro–caspase 2 cleavage in both P4 and P15 WT and *dt*^{27} DRGs. Caspase 2 cleavage in (G) P4 and (H) P15 WT and *dt*^{27} DRGs was quantified by densitometry and normalized to tubulin standard; Student's *t* test, *$p < 0.05$, n = 5.

Western analysis of F11 neuronal cells treated with various concentrations of salubrinal confirmed that it inhibits downstream UPR signaling by preventing dephosphorylation of eIF2α (Figure 8C). Fold change in ethidium homodimer incorporation showed that whereas dystonin-a2 depletion causes a significant increase in death, salubrinal treatment significantly reduces this death (Figure 8, D and E). Finally, we evaluated the effect of salubrinal treatment on viability of *dt*^{27} primary sensory neurons as assessed by ethidium homodimer incorporation. Here we show that UPR blockade with 25 μM salubrinal prevents degeneration in primary *dt*^{27} sensory neurons. In summary, these data highlight a critical role for dystonin-a2 in mediating normal ER structure and function. Loss of this protein leads to the ER stress and apoptosis that underlie the sensory neurodegeneration observed in *dt*^{27} mice.

DISCUSSION

Mutations in the *Dst* gene that encodes all isoforms of the giant cytoskeletal cross-linking protein dystonin result in sensory neurodegeneration in *dt* mice (Bernier *et al.*, 1995). The consensus regarding this degenerative event is that it arises due to loss of structural organization of cytoskeletal elements (Yang *et al.*, 1996, 1999; Leung *et al.*, 1999a). The numerous functions of the cytoskeleton have made elucidation of the mechanism underlying *dt* pathogenesis challenging. Here we identify a signaling cascade resulting from dystonin deficiency in sensory neurons by which loss of organelle integrity that

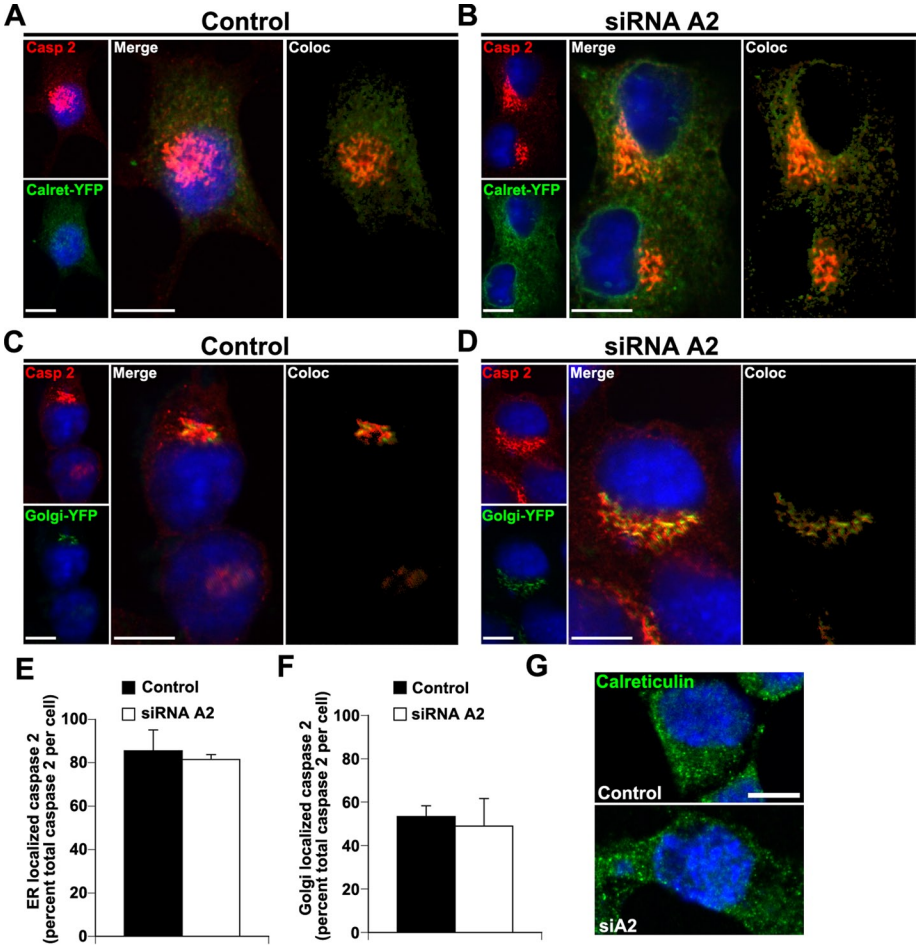

FIGURE 5: Caspase 2 is ER associated in F11 neuronal cells. F11 cells overexpressing either calreticulin-YFP (A, B) or Golgi-YFP (C, D) were antigenically labeled for caspase 2 following 48-h treatment with either (A, C) control or (B, D) dystonin-a2 siRNAs (scale bars, 10 μm). Colocalization of caspase 2 with either the ER (calreticulin) or Golgi was subsequently determined and colocalization masks generated. Quantification of the percentage colocalized area between caspase 2 and (E) the ER or caspase 2 and (F) the Golgi was subsequently performed; Student's *t* test, n = 12. Loss of dystonin has no effect on localization. (G) ER macrostructure was visualized by antigenic labeling of endogenous calreticulin (scale bars, 10 μm). Loss of dystonin-a2 had little effect on calreticulin subcellular organization.

precedes phenotypic onset in dt^{27} mice triggers ER-mediated apoptosis (Figure 9). We observe ultrastructural dilation of the ER that correlates with Ca^{2+} dyshomeostasis and activation of canonical ER stress proteins. This in turn leads to activation of ER stress caspases 2 and 12, culminating in apoptosis. Furthermore, we propose these pathologies to be the consequence of specific loss of dystonin-a2.

Dystonin as a regulator of ER stress

The ER is involved in transduction of apoptotic signaling through two pathways—UPR and Ca^{2+} mobilization. UPR is initiated to restore protein folding in the ER and can itself lead to ER dilation through autophagy (Hoyer-Hansen and Jaattela, 2007). Apoptosis is initiated when ER function cannot be restored (Hoyer-Hansen and Jaattela, 2007). Ca^{2+} mobilization from the ER results in activation of the cysteine protease *m*-calpain (Orrenius *et al.*, 2003). Calpain activation promotes apoptosis through activation of ER-associated caspase 12 (Nakagawa and Yuan, 2000). Alternatively, activation of caspase 2 depends on both cleavage and phosphorylation by Ca^{2+}-dependent CaMKII (Nutt *et al.*, 2005). Caspase 2 propagates apoptosis through activation of executioner caspases and cleavage of cytoskeletal linker protein αII-spectrin. In *dt*, we find a pronounced neuroprotection effected by caspase blockade and a partial rescue of neuronal viability by the UPR inhibitor salubrinal. The dependence of caspase 2 and 12 activation on Ca^{2+} signal transduction implicates ER-Ca^{2+} dyshomeostasis as a primary inducer of neurodegeneration in *dt*.

Molecular interaction studies implicated dystonin in regulation of the dynein motor complex (DMC) through interaction with dynactin and the endosomal vesicle protein retrolinkin (Liu *et al.*, 2003, 2007). It is intriguing to speculate how this interaction may implicate cytoskeletal linker proteins as master regulators of ER function. Mutations in the cytoskeletal linker protein βIII-spectrin cause severe cerebrospinal ataxia in murine and *Drosophila* models (Lorenzo *et al.*, 2010; Perkins *et al.*, 2010). The ataxic phenotype is enhanced by both dynein and dynactin loss-of-function mutations, implicating aberrant intracellular transport as a mediator of pathology (Lorenzo *et al.*, 2010). The potential role for dystonin as a DMC component, coupled with our findings of a role for dystonin-a2 as mediator of ER integrity, supports the notion that dystonin may regulate components of the endocytic pathway. Indeed, cytoskeletal linkers may have a general role in mediating axonal transport by regulating ER and endosomal organization. As such, their dysfunction may contribute to numerous neurodegenerative conditions whose etiologies are unknown. Aberrations in the signaling events described previously are associated with neurodegenerative disease. For example, mutations in the ER protein presenilin-1 found in familial Alzheimer disease (Sherrington *et al.*, 1995) result in aberrant Aβ processing (Lemere *et al.*, 1996) and increased neuronal susceptibility to ER stress (Katayama *et al.*, 1999). ER stress further promotes Aβ generation, propagating disease pathology (Suh and Checler, 2002). Aβ itself mediates ER collapse by interfering with membrane anchoring to the cytoskeleton (Lai *et al.*, 2009).

Dystonin-a2 and organelle integrity

Initial studies on *dt* mice demonstrated an involvement of the perikaryon of certain sensory neurons in disease. Peripheral displacement of Nissl substance, nuclear eccentricity, and cell enlargement were among defects noted (Duchen *et al.*, 1964; Messer and Strominger, 1980; Sotelo and Guenet, 1988). More recently, investigation of dt^{Tg4} sensory neurons also documented perikaryal defects, suggesting that abnormalities other than those from cytoskeletal disorganization in the axon could initiate or contribute to *dt* pathogenesis (Young and Kothary, 2008). These initial observations of *dt* perikaryon abnormalities fit well with recent data that demonstrated an N-terminal transmembrane domain contained in dystonin-a2 facilitates its localization to perinuclear membranes (Young *et al.*, 2006). Involvement of

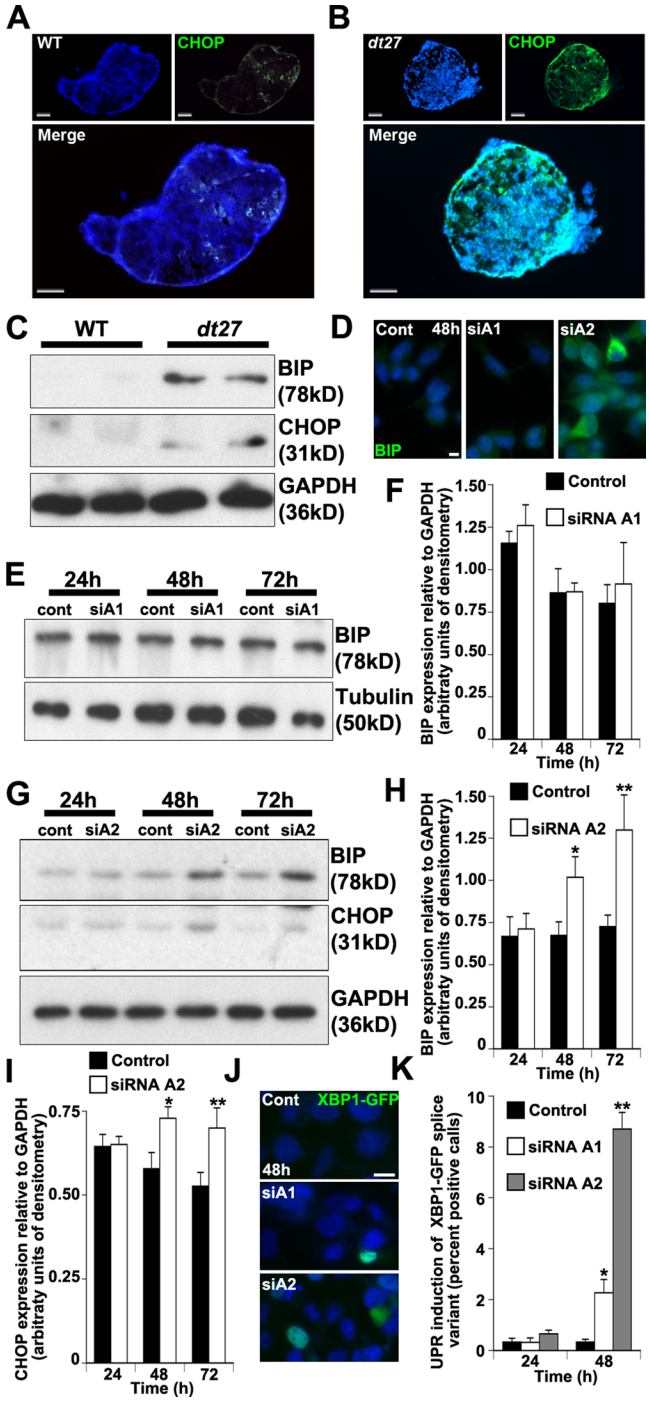

FIGURE 6: Loss of dystonin results in ER stress–mediated induction of the unfolded protein response. (A, B) Antigenic labeling of CHOP by immunofluorescence confirmed an induction of CHOP expression in whole DRGs from *dt*^{27} animals relative to WT littermate controls (scale bars, 50 μm). (C) Phenotypic WT and *dt*^{27} DRGs were analyzed by Western blot for induction of UPR proteins BiP and CHOP. A significant induction of both BiP and CHOP was observed in P15 *dt*^{27} DRGs (each lane represents pooled DRGs from three animals). (D) Induction of BiP expression following loss of dystonin-a2 was confirmed by immunofluorescence antigenic labeling (scale bars, 10 μm). (E–I) Isoform-specific depletion of dystonin was performed in F11 neuronal cells and the effect on UPR induction determined. (E, F) Although Western analysis did not reveal a change in BiP expression following dystonin-a1 silencing, an increase in (G, H) BiP and (G, I) CHOP expression was detected within 48 h of dystonin-a2 silencing; ANOVA, post hoc Dunnett's *t* test, *$p < 0.05$, **$p < 0.01$, $n = 3–7$). (J, K) UPR-mediated activation of XBP1 splicing was then determined by total cell counts of XBP1-GFP expression. A 48-h dystonin-a1 depletion resulted in a modest induction of XBP1 splicing, whereas a dramatic increase in splicing was observed following loss of dystonin-a2 (scale bars, 10 μm); ANOVA, post hoc Dunnett's *t* test, *$p < 0.05$, **$p < 0.01$, $n = 3–7$.

dystonin-a2 as a structural component of the ER is further supported by the finding that ectopic overexpression of dystonin-a2 fusion protein alters the subcellular localization of calreticulin (Young and Kothary, 2008). Furthermore, altered protein disulfide isomerase expression in *dt*^{Tg4} sensory neurons suggested that ER dysfunction or impaired protein folding may come as a result of perturbed ER structure in multiple *dt* mutant alleles (Young and Kothary, 2008).

In the present study, we find ER structural integrity to be perturbed in *dt*^{27} sensory neurons (Figure 7C). Although past studies on *dt* sensory neurons highlighted unexplained changes in ER resident proteins, a mechanistic link between aberrant ER ultrastructure, and activation of ER stress signaling cascades has yet to be resolved. ER dilation and vacuole formation can occur as a component of autophagy and is often induced by ER stress as a neuroprotective mechanism to remove damaged organelles (Marino *et al.*, 2011; Scheper *et al.*, 2011). It is surprising that ER dilation in this instance preceded caspase activation (Figure 4) and UPR induction (data not shown). Considering previous related work on the subject, which described dystonin-a2 as an anchor for perinuclear membranes through its attachment of actin microfilaments, we propose compromised organelle structure to result from loss of cytoskeletal interaction. Indeed, it has been established that organization, movement, and proper function of organelles are highly reliant upon the cytoskeleton (Barr and Egerer, 2005; Starr, 2007; Bola and Allan, 2009). An example of organelle integrity being maintained through cytoskeletal linking proteins is found in the microtubule actin cross-linking factor-1b (MACF1b). As a member of the plakin protein family, MACF1b shares similar domain architecture as dystonin-a. It interacts with microfilaments and microtubules and is critical for Golgi complex polarization and stability of the microtubule-organizing complex (Leung *et al.*, 1999b; Kodama *et al.*, 2003; Lin *et al.*, 2005). Although the two proteins are expressed in many of the same tissues, DRG neurons express predominantly dystonin (Leung *et al.*, 2001), which might explain why *dt* degeneration is most prominent in sensory neurons.

Because the functions of organelles are contingent upon organelle structure, the establishment of dystonin-a2 as an ER structural anchor makes it not surprising that Ca^{2+} dyshomeostasis and UPR activation are observed in *dt* sensory neurons. Hallmark pathologies of many neurodegenerative diseases center on elements of ER dysfunction. Future studies should aim to determine whether abnormal ER morphology causes Ca^{2+} dyshomeostasis, whether dystonin-a2 interacts with ER-proteins, or whether cytoskeletal stabilization prevents ER stress in other sensory neuropathies. The partial rescue implied by UPR blockade following dystonin-a2 loss indicates that the mechanisms causing death of *dt* sensory neurons are still active. To further discern the functions of dystonin isoforms, we must target upstream of ER defects. Collectively, data presented here provide compelling evidence that dystonin-a2 is a critical mediator of normal ER structure and function.

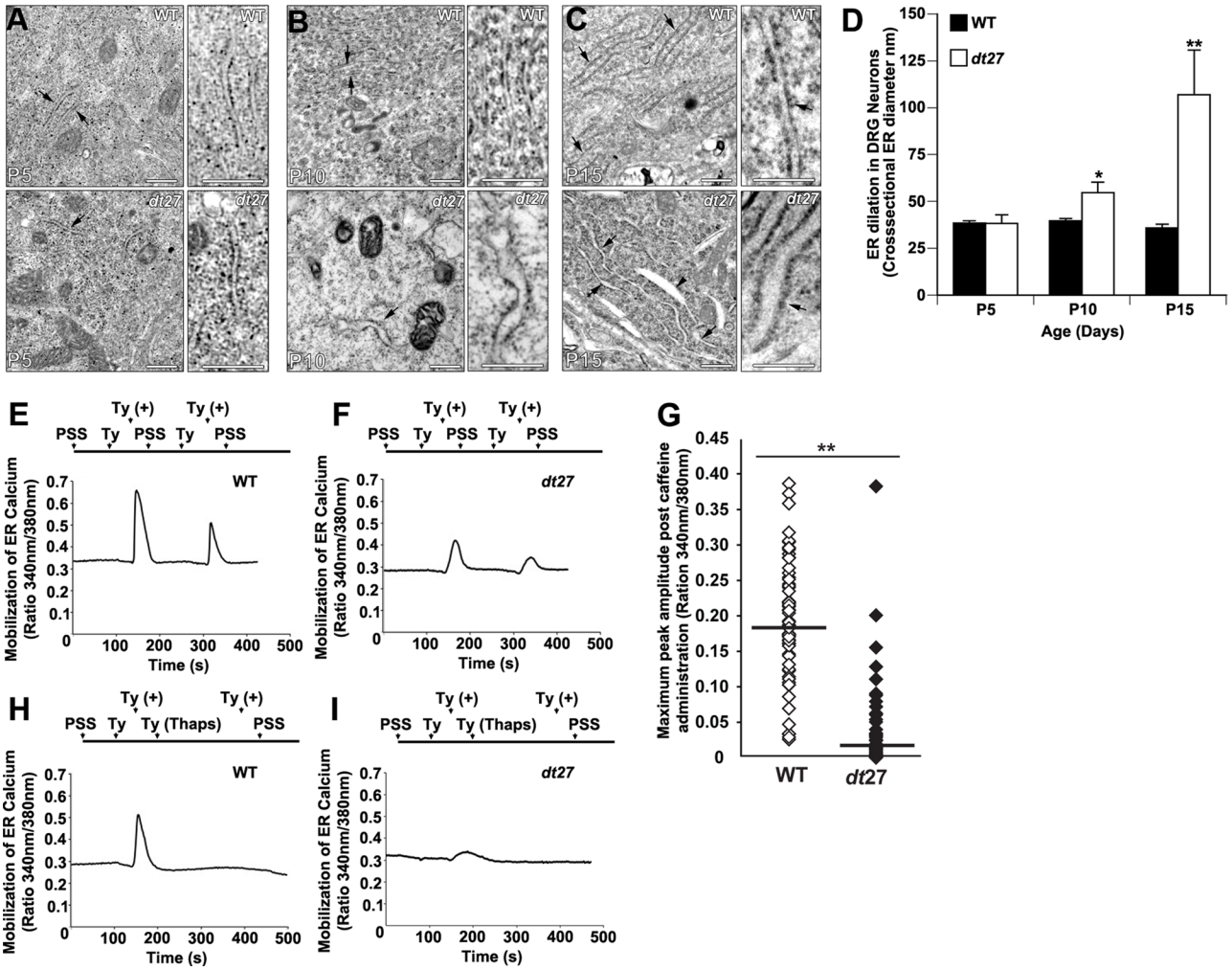

FIGURE 7: ER Ca^{2+} homeostasis is perturbed in the sensory neurons of *dt27* mice. Electron microscopy of WT and *dt*^{27} DRGs at (A) P5, (B) P10, and (C) P15. Normal striated patterning of ER can be observed in WT DRGs (A–C top, arrows). In contrast, the ER in *dt*^{27} DRGs is dilated (A–C, bottom arrows), leading to vacuole formation in some instances (C, bottom, arrowhead; scale bars, 500 nm). (D) Quantification of ER dilation shows a significant increase in ER dilation at P10 and P15 in *dt*^{27} DRGs relative to WT; one-way Student's *t* test, *p < 0.05, **p < 0.01, n = 3. Ca^{2+} mobilization from the ER of (E) P15 WT and (F) *dt*^{27} primary sensory neurons was visualized and recorded using Fura-2AM dye, and a representative graph is depicted. Neurons were perfused with PSS for 100 s prior to Ca^{2+} depletion in tyrode (Ty) buffer for 30 s. Caffeine was then administered for 30 s in tyrode buffer [Ty(+)] to stimulate Ca^{2+} efflux from the ER. Following Ca^{2+} efflux, neurons were then reperfused in PSS to replenish Ca^{2+} stores and the sequence was repeated. Ca^{2+} efflux from the ER is indicated by a shift in the 340/380-nm ratio of Fura-2 fluorescence emittance. (F, G) *dt*^{27} sensory neurons showed reduced ER calcium efflux relative to WT sensory neurons as indicated by a reduction in maximum peak amplitude following caffeine administration; Student's *t* test, **p < 0.01, n = 61–63. Ca^{2+} reuptake was normal in both WT and *dt*^{27} sensory neurons as indicated by the second peak response. The experimental paradigm in E was repeated in (H) WT and (I) *dt*^{27} sensory neurons, with the exception that between the first and second sequences the neurons were perfused with thapsigargin (Thaps) for 180 s to block Ca^{2+} reuptake by SERCA pumps. Following SERCA inhibition, caffeine stimulation did not result in Ca^{2+} mobilization, confirming that caffeine was indeed stimulating efflux from ER stores alone and that all Ca^{2+} in the ER was effluxed following stimulation with caffeine.

MATERIALS AND METHODS

Reagents

All chemicals were purchased through Sigma-Aldrich (St. Louis, MO), and all cell culture reagents were obtained from Invitrogen (Burlington, Canada), except where indicated.

Animals and cell culture

The *dt*^{27} and *dt*^{Tg4} mutant mice and control littermates were used at prephenotype (P4 and P10) or phenotype stage (P15). The generation of these lines and characterization of the mutation were described previously (Kothary *et al.*, 1988; Brown *et al.*, 1995; Pool *et al.*, 2005). The onset of phenotype was generally assessed by the appearance of clasping of hind limbs after the mice were picked up by the tails. *dt*^{27} *and dt*^{Tg4} mice were genotyped by PCR amplification of genomic tail DNA. DRG tissue sections of the lumbar spinal cord region were prepared as previously described (Young and Kothary, 2008). All animal procedures were performed in accordance with institutional guidelines (Animal Care and Veterinary Services and Ethics, University of Ottawa).

Cos-1 cells (an African green monkey kidney fibroblast-like cell line obtained from American Type Culture Collection, Manassas,

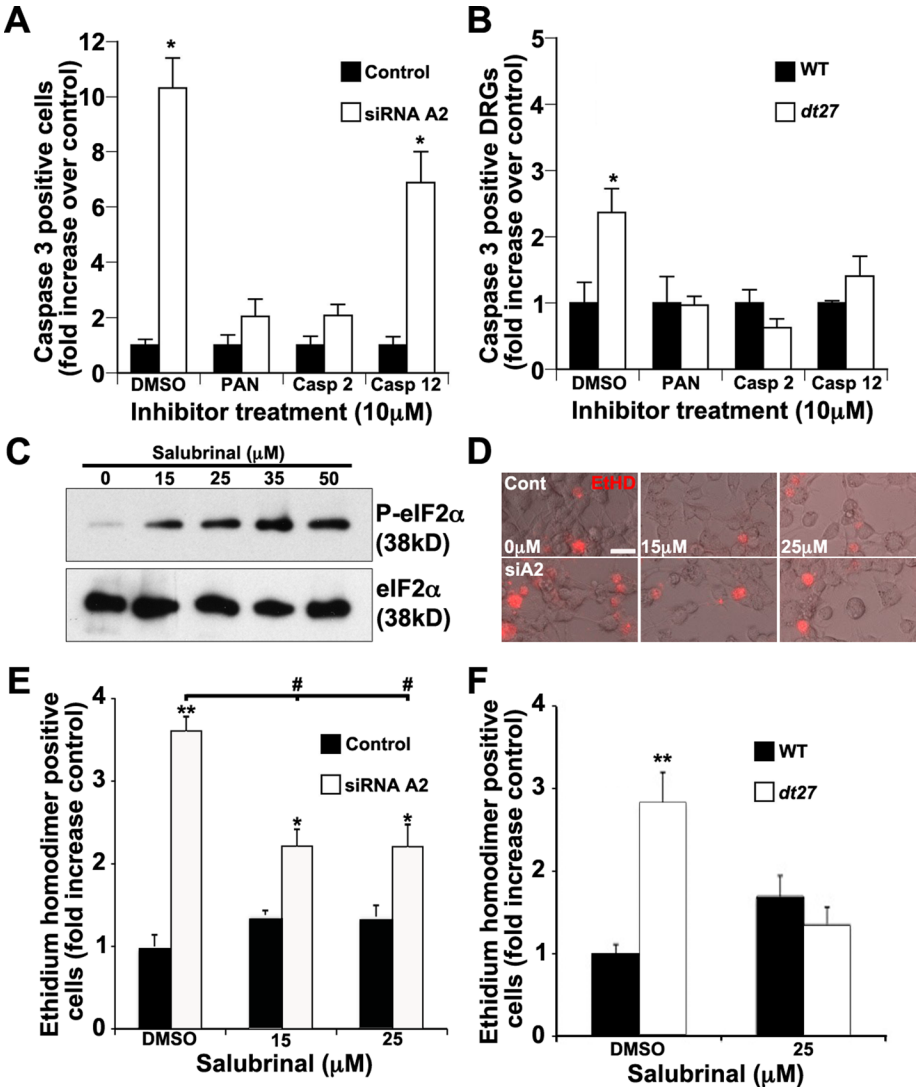

FIGURE 8: Inhibition of ER stress and the associated caspase cascade rescues dystonin-a2–deficient neurons from death. (A) F11 neuronal cells were screened for caspase 3 activation following knockdown of dystonin-a2 in the presence of various caspase inhibitors using the FLICA assay. Pan-caspase inhibition or inhibition of caspase 2 but not caspase 12 prevented downstream caspase 3 activation in F11 neuronal cells; ANOVA, post hoc Dunnett's *t* test, *p < 0.05. (B) In P15 primary sensory neurons from *dt*^{27} mice subjected to the same assay, pan-caspase inhibition in addition to inhibition of either caspase 2 or caspase 12 prevented downstream caspase 3 activation; ANOVA, post hoc Dunnett's *t* test, *p < 0.05, n = 9. (C) Western analysis of F11 neuronal cells treated with various concentrations of salubrinal confirmed that salubrinal inhibits downstream UPR signaling by preventing dephosphorylation of eIF2α. Fold change in ethidium homodimer incorporation showed that whereas dystonin-a2 depletion causes a significant increase in death (ANOVA, post hoc Tukey, **p < 0.01, n = 9), salubrinal treatment at 15 and 25 μM significantly reduces death resulting from depletion of dystonin-A2 in F11 neuronal cells relative to vehicle (DMSO)-treated cells (D, E) (scale bars, 10 μm; ANOVA, post hoc Tukey, #p < 0.05). (F) Measurements of fold change in ethidium homodimer incorporation indicate that 25 μM salubrinal treatment rescues *dt*^{27} primary sensory neurons from death; Student's *t* test, **p < 0.01, n = 18–20.

VA) and F11 cells (a fusion of embryonic rat DRG cells with a mouse neuroblastoma cell line, kindly supplied by Paul Albert, University of Ottawa) were maintained in DMEM + 10% fetal bovine serum (FBS) and 1% penicillin/streptomycin/antimycotic. Cells were passaged at ~70% confluency in 10-cm plastic Petri dishes and plated onto glass coverslips for use in immunofluorescence assays. Cell transfections were performed using Lipofectamine 2000 (Invitrogen), according to the manufacturer's directions.

Primary culture of sensory neurons

Spinal columns were removed from P4, P10, or P15 mice and transferred to a dissection microscope. Approximately 40 DRGs were isolated per mouse and subsequently digested for 15 min each with collagenase A (Roche, Laval, Canada) and papain (Worthington, Lakewood, NJ) solutions. DRG neurons were dissociated with flame-polished glass Pasteur pipettes and seeded onto 12-mm laminin-2 (Millipore, Billerica, MA)–coated coverslips at a density of 50,000 in DMEM with 10% FBS and 1% penicillin/streptomycin. Cells were placed in a 37°C tissue culture incubator under 8.5% CO_2. The following day, the media was changed to neuronal maintenance media (DMEM base, 0.5% FBS, 2% B27, 1% GlutaMax, 16 μg/ml putrescine, 400 μg/ml thyroxine, 400 μg/ml triiodothyronine, 6.2 ng/ml progesterone, 5 ng/ml sodium selenite, 100 μg/ml bovine albumin serum, 5 μg/ml bovine insulin, 50 μg/ml holotransferrin) supplemented with 200 ng/ml nerve growth factor and 1 μM 5-fluoro-2′-deoxyuridine. A three-fourths media change was carried out every other day, up until day 6 of culture, when calcium-imaging experiments were performed.

Sample preparation for electron microscopy

Samples for electron microscopy were prepared as previously described (De Repentigny *et al.*, 2011). Briefly, *dt*^{27J} (n = 4) and WT (n = 4) mice were anesthetized at P5, P10, or P15 via intraperitoneal injection of tribromoethanol (Avertin). Mice were perfused transcardially with 3 ml of phosphate-buffered saline (PBS), followed by 10 ml of Karnovsky's fixative (4% paraformaldehyde [PFA], 2% glutaraldehyde, and 0.1 M cacodylate buffer in PBS, pH 7.4). The lumbar region of the spinal cord was dissected and DRGs collected under a stereomicroscope. Ultrathin sections (70 nm) were placed on a 300-mesh copper specimen grid, counterstained in 5% uranyl acetate and Reynold's lead citrate, and then observed by transmission electron microscopy.

siRNA and RT-PCR

Custom siRNAs were developed to target specific dystonin isoforms. To knock down dystonin-a1 and dystonin-a2, isoform-specific nucleotides between 2310 and 2380 (accession number AF396878) for dystonin-a1 and nucleotides between 1 and 661 (accession number: DQ02331) for dystonin-a2 were chosen for the development of siRNAs. The following groups of siRNA sequences were efficacious in knocking down dystonin-a1 and dystonin-a2 expression, respectively: group A (sense 5′–3′) ACAUGUACGUGGAGGAGCAtt; (antisense 5′–3′) UGCUCCUCCACGUACAUGUag, (sense 5′–3′) CCGCCUACAUGUACGUGGAtt

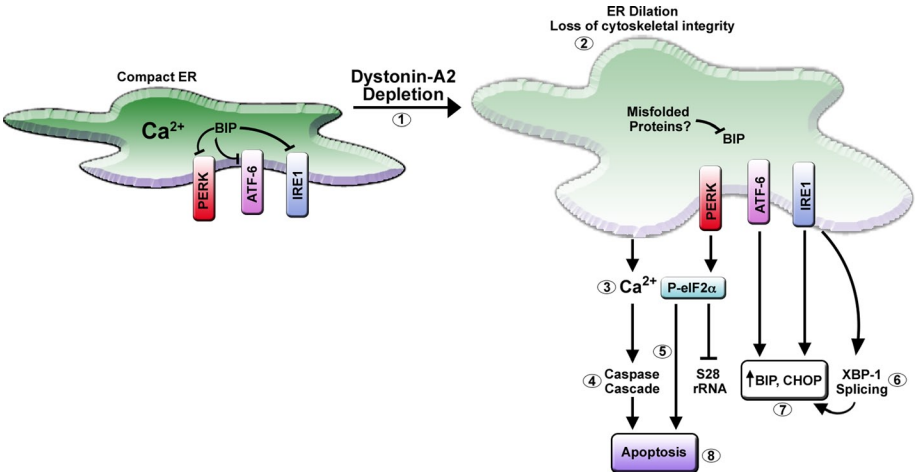

FIGURE 9: Proposed model of apoptotic signaling initiated by depletion of dystonin-a2 in sensory neurons. 1) Schematic representation of the events that occur following depletion of dystonin-a2 in sensory neurons. 2) Depletion of dystonin-a2 results in a loss of cytoskeletal integrity that culminates in dilation of the ER. 3) Perturbed ER homeostasis leads to a decrease in the steady-state levels of Ca^{2+} in the ER. 4) The associated rise in free intracellular Ca^{2+} likely results in activation of an ER-dependent caspase cascade, inhibition of which can maintain cell viability. 5) Blockade of downstream eIF2α signaling with salubrinal partially rescues neurodegeneration following dystonin-a2 depletion, implicating PERK-mediated eIF2α signal transduction in the apoptotic cascade. 6) Enhanced XBP1 splicing likely coupled with activation of ATF-6 and IRE1 promotes expression of protein chaperones (7) BiP and CHOP in an attempt to maintain ER function. 8) The inability to rescue ER structural integrity culminates in DNA cleavage and programmed cell death.

(antisense 5′–3′) UCCACGUACAUGUAGGCGGcg; group B (sense 5′–3′) CAAGCAUGAGAGAUCCAAAtt; (antisense 5′–3′) UUUGGAUCUCUCAUGCUUGgg; (sense 5′–3′) CUUCCUCUUGUUGCUCCUGtt; (antisense 5′–3′) CAGGAGCAACAAGAGGAAGag. The siRNA target sequences were conserved between mouse and rat. All siRNAs (Silencer Select Custom Designed siRNA) were obtained from Applied Biosystems/Ambion (Austin, TX) and compared with the effects of scrambled controls matched for GC content. F11 and Cos-1 cells were transfected with siRNA using Lipofectamine 2000. Knockdown was assessed at the transcript and protein level. Total RNA was collected from F11 cells using RNeasy Mini Kit (Qiagen, Toronto, Canada) according to manufacturer's protocol. For RT-PCR, QuantiTect Reverse Transcription Kit (Qiagen) was used, following manufacturer's protocol. cDNAs encoding dystonin-a1, dystonin-a2, and actin (control) derived from mouse were PCR amplified as previously described (Pool *et al.*, 2005). For assessment of protein knockdown, Cos-1 cells were cotransfected with siRNA and recombinant dystonin proteins (dystonin-a2–YFP and Nterm-dystonin-a1–GFP) using Lipofectamine 2000. Fluorescence intensity of recombinant dystonin proteins was used to assess siRNA knockdown efficiency.

Recombinant proteins

The dystonin-a1–GFP construct (GFP-Nterm1) was previously described (Young *et al.*, 2003). The dystonin-a2–YFP construct was designed and cloned by Kevin Young while a member of the Kothary lab. The 5′ N-terminal region of the dystonin-a2 isoform (a2Ntermmyc/his; Young and Kothary, 2008) and the 3′ end of an expressed sequence tag clone (GenBank accession AI526522; Young *et al.*, 2006) were ligated in frame into a pEYFP-N1 vector. The reporter plasmid pHA-XBP1u-GFP was a gift from John Ngsee of the Ottawa Hospital Research Institute and was previously described (Yu *et al.*, 2006). Calreticulin-YFP and Golgi-YFP were gifts from Xiaohui Zha of the Ottawa Hospital Research Institute.

Cell viability

Dead cells were identified by uptake of ethidium homodimer (2 μM) as a result of loss of membrane integrity. Cells were then visualized with a Zeiss Axiovert 200m epifluorescence microscope under 10× objective (Achroplan 0.25) equipped with an AxioCam HRM digital camera and AxioVision 4.6 software (Zeiss, Toronto, Canada).

Fluoro-Jade B staining

Fluoro-Jade B (Millipore) staining was performed according to the method of Schmued *et al.* (1997). Briefly, 12-μm DRG sections were fixed with 4% PFA dried on a slide warmer at 45°C. The tissue was then subjected to a series of washes (100% ethanol, 3 min; 70% ethanol, 1 min; ddH_2O, 1 min; 0.06% potassium permanganate, 15 min; double-distilled water, 1 min; 0.001% Fluoro-Jade in 0.1% acetic acid, 20 min; 3× double-distilled water, 1 min; and xylene, 1 min; and then coverslipped with Permount [Fisher Scientific, Ottawa, Canada]). Sections were analyzed with a Zeiss Axiovert 200m epifluorescence microscope under 10× objective (Achroplan 0.25) equipped with an AxioCam HRM digital camera and AxioVision 4.6 software.

TUNEL

Cells/tissue was washed in PBS and permeabilized in ice-cold 0.1% sodium citrate/0.1% Triton X-100 for 5 min, followed by 2 min in 2:1 ethanol:acetic acid on ice. Samples were rinsed for 2 min in PBS and incubated for 1 h at 37°C with FITC-labeled dUTP in terminal deoxynucleotidyl transferase (TdT) buffer (30 mM Tris-HCl, pH 7.2, 140 mM sodium cacodylate, and 1 mM cobalt chloride) and TdT according to the protocol provided by the manufacturer (Roche). Negative controls included sections incubated with fluorescein isothiocyanate–labeled dUTP in the absence of TdT. Cells were washed in PBS, mounted in fluorescence mounting media (Dako, Burlington, ON), and analyzed with a Zeiss Axiovert 200m epifluorescence microscope under 10× objective (Achroplan 0.25) equipped with an AxioCam HRM digital camera and AxioVision 4.6 software.

Caspase activity assay

Caspase activity in live cells was measured using fluorescein (caspase 12, fluorescein isothiocyanate–ATAD–fluoromethyl ketone [FMK]; Abcam, Cambridge MA) and fluorescence-labeled inhibitor of caspase activity (FLICA; caspase 8, carboxyfluorescein [FAM]–LETD–FMK; caspase 2, FAM-VDVAD-FMK; and caspase 3/7, FAM-DEVD-FMK; ImmunoChemistry Technologies, Bloomington, MN) assays. Fluorescein/FLICA assays were performed using a modified protocol from the manufacturers' instructions. Briefly, 1.67 μl of 30× fluorescein/FLICA reagent (diluted in PBS) was added to each well of a 96-well plate. Cells were incubated for 1 h at 37°C and 5% CO_2. Cells were washed twice in PBS and analyzed with a Zeiss Axiovert 200m epifluorescence microscope under 10× objective (Achroplan 0.25) equipped with an AxioCam HRM digital camera and AxioVision 4.6 software. Phase contrast and fluorescence photos were taken of six random fields per well for three of four replicate wells in duplicate or triplicate experiments. The mean number of cells with active caspases at each time point was determined, and data were then

standardized against scrambled or WT controls where appropriate to determine fold change in caspase activity attributable to loss of dystonin. Functional dependence of downstream caspase activation on active caspases 2 and 12 or other caspase activation (PAN) was assessed. F11 or primary sensory neurons were treated with either the caspase 2 inhibitor Z-VDVAD-FMK (50 μM), the caspase 12 inhibitor Z-ATAD-FMK (50 μM), or the PAN caspase inhibitor Z-VAD-FMK. Caspase 3 activation was then assessed as described.

Immunocytochemistry

Cultures were fixed in 4% PFA prior to antigenic labeling. Primary antibodies used were rabbit polyclonal anti–cleaved caspase 3 (1:1000; Cell Signaling Technology, Beverly, MA), mouse monoclonal anti–caspase 2 (1:500; EMD Biosciences, San Diego, CA), and mouse monoclonal anti-CHOP (1:1000; Cell Signaling Technologies). Secondary antibodies used were anti–mouse Alexa 488 (1:2000; Molecular Probes, Invitrogen), anti–mouse Alexa 555 (1:2000; Molecular Probes), and anti–rabbit Alexa 488 (1:2000; Molecular Probes). Antibodies were diluted in antibody buffer (PBS, 0.3% Triton X-100, 3% BSA). Where 4′,6-diamidino-2-phenylindole (DAPI) staining is indicated, samples were incubated in DAPI stain (0.2 μg/ml in PBS) for 10 min and washed three times in PBS for 5 min. Samples were mounted in fluorescence mounting media (Dako) and analyzed a Zeiss Axiovert 200m epifluorescence microscope under either a 10× objective (Achroplan 0.25) or a 40× objective (Achroplan 1.3 Oil) equipped with an AxioCam HRM digital camera and AxioVision 4.6 software. Where colocalization studies were performed, F11 neuronal cells treated with either scrambled siRNA or siRNA targeted against dystonin-a2 were analyzed with an LSM 510 meta confocal microscope equipped with an EC Plan-Neofluar 40×/1.30 Oil DIC M27 objective using Zen 8.0 software (Zeiss). Using the colocalization module of Zen 8.0, we compared the total area of caspase 2 staining per the cell with the area of caspase 2 staining that colocalized with either calreticulin-YFP or Golgi-YFP within that same cell. The area of colocalization was then calculated as the percentage colocalized area over the total area of caspase 2. Twelve cells from three different experiments were analyzed per condition.

Western analysis

Proteins were isolated in RIPA buffer (10 mM PBS, 1% NP40, 0.5% sodium deoxycholate, 0.1% SDS, 30 μl/ml aprotinin, 10 mM Na orthovanadate, 100 μl/ml phenylmethylsulfonyl fluoride). Protein samples (30 μg) were separated by SDS–PAGE under reducing conditions. Western analyses were performed using primary mouse monoclonal anti–caspase 2 (1:500; BD Transduction Laboratories, Lexington, KY), mouse monoclonal anti-CHOP (1:1000, Cell Signaling Technology), polyclonal anti–binding protein (BiP, 1:1000; Cell Signaling Technology), rabbit polyclonal anti–phospho-eIF2α (1:1000; Cell Signaling Technology), rabbit polyclonal anti-eIF2α (1:1000; Cell Signaling Technology), rabbit polyclonal anti– glyceraldehyde-3-phosphate dehydrogenase (GAPDH) (1:5000; Abcam), and mouse monoclonal anti–BIII-tubulin (1:2000, E7 clone; Hybridoma Bank, Iowa City, IA). Owing to low protein yields from DRGs, analysis of ER stress (Figure 6 and Supplemental Figure S2) was performed using pooled DRGs from three WT and three *dt*^{27} mice per sample. A 40-μg protein sample was loaded thereafter. Secondary antibodies used were horseradish peroxidase (HRP)–conjugated anti-mouse immunoglobulin G (IgG, 1:2000; Bio-Rad, Hercules, CA) and HRP-conjugated anti–rabbit IgG (1:2000; Bio-Rad). Immunoreactive bands were visualized using SuperSignal West Pico (MJS BioLynx, Brockville, Canada). Quantification of protein expression levels was performed by densitometric analysis of individual bands using ImageJ analysis software (National Institutes of Health, Bethesda, MD). At least three Western blots from different experiments were evaluated by densitometry and normalized to a protein standard (actin, tubulin, or GAPDH) for all Western blots depicted.

Ratiometric measurement of intracellular Ca^{2+} using Fura-2AM in primary sensory neurons

The measurement of intracellular Ca^{2+} ($[Ca^{2+}]i$) was performed using the ratiometric dye Fura-2AM based on previously published protocol (Jiang *et al.*, 2005). Briefly, P15 sensory neuron cultures or F11 neuronal cells were grown on 2-mm laminin-2 (Millipore)–coated coverslips (as described) and loaded with 5 μM Fura-2AM (Molecular Probes) and 0.02% pluronic acid in neuronal maintenance media and placed in a 37°C tissue culture incubator under 8.5% CO_2 for 30 min. Sensory neuron cultures were then rinsed with PSS Mg^{2+} buffer (2 mM 4-(2-hydroxyethyl)-1-piperazineethanesulfonic acid [HEPES], pH 7.2, 140 mM NaCl, 5 mM KCl, 2.3 mM $CaCl_2$, and 10 mM glucose) and stabilized in the same buffer for 5 min and then placed in a microperfusion chamber, where Fura-2AM intensities were measured by the Northern Eclipse Digital Ratio Image System (EMPIX, Mississauga, Canada) with an Axiovert 200 camera and light source (Zeiss). After a region was chosen, Fura-2 fluorescence was measured at 510-nm emission with 340/380-nm dual excitation selected by a DG-5 system (Sutter Instrument Company, Novato, CA). $[Ca^{2+}]i$ concentration was determined via the ratio of fluorescence intensity between the two excitation wavelengths of 340/380 nm of Fura-2. The basal level of $[Ca^{2+}]i$ was recorded for 100 s in PSS buffer, followed by a 30-s perfusion of calcium-free Tyrode solution (9 mM NaCl, 12.5 mM KCl, 3 mM $MgCl_2$, 30 mM glucose, 25 mM HEPES, 1 mM ethylene glycol tetraacetic acid, pH 7.4), followed by a 30-s perfusion of Tyrode solution plus caffeine (20 mM). These perfusions were repeated a second time or following 180 s of perfusion with thapsigargin (20 nM) in PSS.

Statistical analysis

Data were analyzed using Student's *t* test or factorial analysis of variance (ANOVA) as applicable using InStat, version 3.0 (GraphPad Software, La Jolla, CA). Following detection of a statistically significant difference in a given series of treatments by ANOVA, post hoc Dunnett's *t* tests or Tukey tests were performed where appropriate. $p < 0.05$ was considered statistically significant (shown as either * or #); $p < 0.01$ was considered highly statistically significant (shown as **).

ACKNOWLEDGMENTS

We thank Kevin Young for creation of the dystonin-a2–YFP construct, as well as Justin Boyer and the rest of the Kothary laboratory for helpful discussions. We thank Michael Rudnicki for comments on the manuscript, Paul Albert for donation of the F11 cell line, Xiaohui Zha for the calreticulin-YFP and Golgi-YFP constructs, and Johnny Ngsee for the pHA-XBP1u-GFP construct. We also thank Robert Monnette for technical assistance with Ca^{2+} imaging. This work was supported by a grant from the Canadian Institutes of Health Research, a Multiple Sclerosis Society of Canada Research Fellowship, and a Canadian Institutes of Health Research Fellowship to S.D.R., with the support of the Dystonia Medical Research Foundation of Canada. T.S. is a Research Fellow of the Japan Society for the Promotion of Science. R.K. is a recipient of a University Health Research Chair from the University of Ottawa.

REFERENCES

Barr FA, Egerer J (2005). Golgi positioning: are we looking at the right MAP? J Cell Biol 168, 993–998.

Bernier G, Brown A, Dalpe G, De Repentigny Y, Mathieu M, Kothary R (1995). Dystonin expression in the developing nervous system predominates in the neurons that degenerate in dystonia musculorum mutant mice. Mol Cell Neurosci 6, 509–520.

Bernier G, De Repentigny Y, Mathieu M, David S, Kothary R (1998). Dystonin is an essential component of the Schwann cell cytoskeleton at the time of myelination. Development 125, 2135–2148.

Bernier G, Kothary R (1998). Prenatal onset of axonopathy in dystonia musculorum mice. Dev Genet 22, 160–168.

Bola B, Allan V (2009). How and why does the endoplasmic reticulum move? Biochem Soc Trans 37, 961–965.

Boyce M *et al.* (2005). A selective inhibitor of eIF2alpha dephosphorylation protects cells from ER stress. Science 307, 935–939.

Brown A, Bernier G, Mathieu M, Rossant J, Kothary R (1995). The mouse dystonia musculorum gene is a neural isoform of bullous pemphigoid antigen 1. Nat Genet 10, 301–306.

Cheung HH, Lynn Kelly N, Liston P, Korneluk RG (2006). Involvement of caspase-2 and caspase-9 in endoplasmic reticulum stress-induced apoptosis: a role for the IAPs. Exp Cell Res 312, 2347–2357.

Dalpe G, Leclerc N, Vallee A, Messer A, Mathieu M, De Repentigny Y, Kothary R (1998). Dystonin is essential for maintaining neuronal cytoskeleton organization. Mol Cell Neurosci 10, 243–257.

Dalpe G, Mathieu M, Comtois A, Zhu E, Wasiak S, De Repentigny Y, Leclerc N, Kothary R (1999). Dystonin-deficient mice exhibit an intrinsic muscle weakness and an instability of skeletal muscle cytoarchitecture. Dev Biol 210, 367–380.

De Repentigny Y, Deschenes-Furry J, Jasmin BJ, Kothary R (2003). Impaired fast axonal transport in neurons of the sciatic nerves from dystonia musculorum mice. J Neurochem 86, 564–571.

De Repentigny Y, Ferrier A, Ryan SD, Sato T, Kothary R (2011). Motor unit abnormalities in dystonia musculorum mice. PLoS ONE 6, e21093.

Dowling J, Yang Y, Wollmann R, Reichardt LF, Fuchs E (1997). Developmental expression of BPAG1-n: insights into the spastic ataxia and gross neurologic degeneration in dystonia musculorum mice. Dev Biol 187, 131–142.

Duchen LW (1976). Dystonia musculorum—an inherited disease of the nervous system in the mouse. Adv Neurol 14, 353–365.

Duchen LW, Strich SJ, Falconer DS (1964). Clinical and pathological studies of an hereditary neuropathy in mice (dystonia musculorum). Brain 87, 367–378.

Ehrlich BE, Kaftan E, Bezprozvannaya S, Bezprozvanny I (1994). The pharmacology of intracellular Ca(2+)-release channels. Trends Pharmacol Sci 15, 145–149.

Eyer J, Cleveland DW, Wong PC, Peterson AC (1998). Pathogenesis of two axonopathies does not require axonal neurofilaments. Nature 391, 584–587.

Ferri KF, Kroemer G (2001). Organelle-specific initiation of cell death pathways. Nat Cell Biol 3, E255–E263.

Fuchs E, Karakesisoglou I (2001). Bridging cytoskeletal intersections. Genes Dev 15, 1–14.

Giorda R *et al.* (2004). Selective disruption of muscle and brain-specific BPAG1 isoforms in a girl with a 6;15 translocation, cognitive and motor delay, and tracheo-oesophageal atresia. J Med Genet 41, e71.

Gulow K, Bienert D, Haas IG (2002). BiP is feed-back regulated by control of protein translation efficiency. J Cell Sci 115, 2443–2452.

Guo L, Degenstein L, Dowling J, Yu QC, Wollmann R, Perman B, Fuchs E (1995). Gene targeting of BPAG1: abnormalities in mechanical strength and cell migration in stratified epithelia and neurologic degeneration. Cell 81, 233–243.

Hitomi J *et al.* (2004). Involvement of caspase-4 in endoplasmic reticulum stress-induced apoptosis and Abeta-induced cell death. J Cell Biol 165, 347–356.

Hoyer-Hansen M, Jaattela M (2007). Connecting endoplasmic reticulum stress to autophagy by unfolded protein response and calcium. Cell Death Differ 14, 1576–1582.

Janota I (1972). Ultrastructural studies of an hereditary sensory neuropathy in mice (dystonia musculorum). Brain 95, 529–536.

Jefferson JJ, Leung CL, Liem RK (2006). Dissecting the sequence specific functions of alternative N-terminal isoforms of mouse bullous pemphigoid antigen 1. Exp Cell Res 312, 2712–2725.

Jiang SX, Lertvorachon J, Hou ST, Konishi Y, Webster J, Mealing G, Brunette E, Tauskela J, Preston E (2005). Chlortetracycline and demeclocycline inhibit calpains and protect mouse neurons against glutamate toxicity and cerebral ischemia. J Biol Chem 280, 33811–33818.

Katayama T *et al.* (1999). Presenilin-1 mutations downregulate the signalling pathway of the unfolded-protein response. Nat Cell Biol 1, 479–485.

Kodama A, Karakesisoglou I, Wong E, Vaezi A, Fuchs E (2003). ACF7: an essential integrator of microtubule dynamics. Cell 115, 343–354.

Kothary R, Clapoff S, Brown A, Campbell R, Peterson A, Rossant J (1988). A transgene containing lacZ inserted into the dystonia locus is expressed in neural tube. Nature 335, 435–437.

Lai CS, Preisler J, Baum L, Lee DH, Ng HK, Hugon J, So KF, Chang RC (2009). Low molecular weight Abeta induces collapse of endoplasmic reticulum. Mol Cell Neurosci 41, 32–43.

Lee AH, Iwakoshi NN, Glimcher LH (2003). XBP-1 regulates a subset of endoplasmic reticulum resident chaperone genes in the unfolded protein response. Mol Cell Biol 23, 7448–7459.

Lemere CA *et al.* (1996). The E280A presenilin 1 Alzheimer mutation produces increased A beta 42 deposition and severe cerebellar pathology. Nat Med 2, 1146–1150.

Leung CL, Sun D, Liem RK (1999a). The intermediate filament protein periperin is the specific interaction partner of mouse BPAG1-n (dystonin) in neurons. J Cell Biol 144, 435–446.

Leung CL, Sun D, Zheng M, Knowles DR, Liem RK (1999b). Microtubule actin cross-linking factor (MACF): a hybrid of dystonin and dystrophin that can interact with the actin and microtubule cytoskeletons. J Cell Biol 147, 1275–1286.

Leung CL, Zheng M, Prater SM, Liem RK (2001). The BPAG1 locus: alternative splicing produces multiple isoforms with distinct cytoskeletal linker domains, including predominant isoforms in neurons and muscles. J Cell Biol 154, 691–697.

Lin CM, Chen HJ, Leung CL, Parry DA, Liem RK (2005). Microtubule actin crosslinking factor 1b: a novel plakin that localizes to the Golgi complex. J Cell Sci 118, 3727–3738.

Liu JJ, Ding J, Kowal AS, Nardine T, Allen E, Delcroix JD, Wu C, Mobley W, Fuchs E, Yang Y (2003). BPAG1n4 is essential for retrograde axonal transport in sensory neurons. J Cell Biol 163, 223–229.

Liu JJ, Ding J, Wu C, Bhagavatula P, Cui B, Chu S, Mobley WC, Yang Y (2007). Retrolinkin, a membrane protein, plays an important role in retrograde axonal transport. Proc Natl Acad Sci USA 104, 2223–2228.

Lorenzo DN, Li MG, Mische SE, Armbrust KR, Ranum LP, Hays TS (2010). Spectrin mutations that cause spinocerebellar ataxia type 5 impair axonal transport and induce neurodegeneration in *Drosophila*. J Cell Biol 189, 143–158.

Lytton J, Westlin M, Hanley MR (1991). Thapsigargin inhibits the sarcoplasmic or endoplasmic reticulum Ca-ATPase family of calcium pumps. J Biol Chem 266, 17067–17071.

Mancini M, Machamer CE, Roy S, Nicholson DW, Thornberry NA, Casciola-Rosen LA, Rosen A (2000). Caspase-2 is localized at the Golgi complex and cleaves golgin-160 during apoptosis. J Cell Biol 149, 603–612.

Marino G, Madeo F, Kroemer G (2011). Autophagy for tissue homeostasis and neuroprotection. Curr Opin Cell Biol 23, 198–206.

Messer A, Strominger NL (1980). An allele of the mouse mutant dystonia musculorum exhibits lesions in red nucleus and striatum. Neuroscience 5, 543–549.

Munro S, Pelham HR (1986). An Hsp70-like protein in the ER: identity with the 78 kd glucose-regulated protein and immunoglobulin heavy chain binding protein. Cell 46, 291–300.

Murakami Y, Aizu-Yokota E, Sonoda Y, Ohta S, Kasahara T (2007). Suppression of endoplasmic reticulum stress-induced caspase activation and cell death by the overexpression of Bcl-xL or Bcl-2. J Biochem 141, 401–410.

Nakagawa T, Yuan J (2000). Cross-talk between two cysteine protease families. Activation of caspase-12 by calpain in apoptosis. J Cell Biol 150, 887–894.

Nakagawa T, Zhu H, Morishima N, Li E, Xu J, Yankner BA, Yuan J (2000). Caspase-12 mediates endoplasmic-reticulum-specific apoptosis and cytotoxicity by amyloid-beta. Nature 403, 68–103.

Nutt LK, Margolis SS, Jensen M, Herman CE, Dunphy WG, Rathmell JC, Kornbluth S (2005). Metabolic regulation of oocyte cell death through the CaMKII-mediated phosphorylation of caspase-2. Cell 123, 89–103.

Okumura M, Yamakawa H, Ohara O, Owaribe K (2002). Novel alternative splicings of BPAG1 (bullous pemphigoid antigen 1) including the domain structure closely related to MACF (microtubule actin cross-linking factor). J Biol Chem 277, 6682–6687.

Orrenius S, Zhivotovsky B, Nicotera P (2003). Regulation of cell death: the calcium-apoptosis link. Nat Rev Mol Cell Biol 4, 552–565.

Ouasti S, Matarrese P, Paddon R, Khosravi-Far R, Sorice M, Tinari A, Malorni W, Degli Esposti M (2007). Death receptor ligation triggers membrane scrambling between Golgi and mitochondria. Cell Death Differ 14, 453–461.

Perkins EM *et al.* (2010). Loss of beta-III spectrin leads to Purkinje cell dysfunction recapitulating the behavior and neuropathology of spinocerebellar ataxia type 5 in humans. J Neurosci 30, 4857–4867.

Platika D, Boulos MH, Baizer L, Fishman MC (1985). Neuronal traits of clonal cell lines derived by fusion of dorsal root ganglia neurons with neuroblastoma cells. Proc Natl Acad Sci USA 82, 3499–3503.
Pool M, Boudreau Lariviere C, Bernier G, Young KG, Kothary R (2005). Genetic alterations at the Bpag1 locus in dt mice and their impact on transcript expression. Mamm Genome 16, 909–917.
Pool M, Rippstein P, McBride H, Kothary R (2006). Trafficking of macromolecules and organelles in cultured dystonia musculorum sensory neurons is normal. J Comp Neurol 494, 549–558.
Sawamura D, Li K, Chu ML, Uitto J (1991). Human bullous pemphigoid antigen (BPAG1). Amino acid sequences deduced from cloned cDNAs predict biologically important peptide segments and protein domains. J Biol Chem 266, 17784–17790.
Scheper W, Nijholt DA, Hoozemans JJ (2011). The unfolded protein response and proteostasis in Alzheimer disease: preferential activation of autophagy by endoplasmic reticulum stress. Autophagy 7, 910–911.
Schmued LC, Albertson C, Slikker W Jr (1997). Fluoro-Jade: a novel fluorochrome for the sensitive and reliable histochemical localization of neuronal degeneration. Brain Res 751, 37–46.
Sherrington R *et al*. (1995). Cloning of a gene bearing missense mutations in early-onset familial Alzheimer's disease. Nature 375, 754–760.
Sonnenberg A, Liem RK (2007). Plakins in development and disease. Exp Cell Res 313, 2189–2203.
Sotelo C, Guenet JL (1988). Pathologic changes in the CNS of dystonia musculorum mutant mouse: an animal model for human spinocerebellar ataxia. Neuroscience 27, 403–424.
Starr DA (2007). Communication between the cytoskeleton and the nuclear envelope to position the nucleus. Mol Biosyst 3, 583–589.
Suh YH, Checler F (2002). Amyloid precursor protein, presenilins, and alpha-synuclein: molecular pathogenesis and pharmacological applications in Alzheimer's disease. Pharmacol Rev 54, 469–525.
Yang Y, Bauer C, Strasser G, Wollman R, Julien JP, Fuchs E (1999). Integrators of the cytoskeleton that stabilize microtubules. Cell 98, 229–238.
Yang Y, Dowling J, Yu QC, Kouklis P, Cleveland DW, Fuchs E (1996). An essential cytoskeletal linker protein connecting actin microfilaments to intermediate filaments. Cell 86, 655–665.
Yoshida H, Matsui T, Yamamoto A, Okada T, Mori K (2001). XBP1 mRNA is induced by ATF6 and spliced by IRE1 in response to ER stress to produce a highly active transcription factor. Cell 107, 881–891.
Young KG, Kothary R (2007). Dystonin/Bpag1—a link to what? Cell Motil Cytoskeleton 64, 897–905.
Young KG, Kothary R (2008). Dystonin/Bpag1 is a necessary endoplasmic reticulum/nuclear envelope protein in sensory neurons. Exp Cell Res 314, 2750–2761.
Young KG, Pinheiro B, Kothary R (2006). A Bpag1 isoform involved in cytoskeletal organization surrounding the nucleus. Exp Cell Res 312, 121–134.
Young KG, Pool M, Kothary R (2003). Bpag1 localization to actin filaments and to the nucleus is regulated by its N-terminus. J Cell Sci 116, 4543–4555.
Yu CY, Hsu YW, Liao CL, Lin YL (2006). Flavivirus infection activates the XBP1 pathway of the unfolded protein response to cope with endoplasmic reticulum stress. J Virol 80, 11868–11880.